Nanoscale

PAPER

View Article Online
View Journal | View Issue

Cite this: *Nanoscale*, 2014, **6**, 2710

Quantum dot-functionalized porous ZnO nanosheets as a visible light induced photoelectrochemical platform for DNA detection

Wenjing Wang,[a] Qing Hao,[a] Wei Wang,[b] Lei Bao,[a] Jianping Lei,*[a] Quanbo Wang[a] and Huangxian Ju[a]

This work reports the synthesis of novel CdTe quantum dot (QD)-functionalized porous ZnO nanosheets *via* a covalent binding method with (3-aminopropyl)triethoxysilane as a linker. The functional nanosheets showed an excellent visible-light absorbency and much higher photoelectrochemical activity than both CdTe QDs and ZnO nanosheets due to the porous structure and appropriate band alignment between the CdTe QDs and ZnO nanosheets. Using hydrogen peroxide as an electron acceptor the nanosheet-modified electrode showed a sensitive photocurrent response. This speciality led to a novel methodology for the design of hydrogen peroxide-related biosensors by the formation or consumption of hydrogen peroxide. Using biotin-labeled DNA as capture probe, a model biosensor was proposed by immobilizing the probe on a nanosheet-modified electrode to recognize target DNA in the presence of an assistant DNA, which produced a "Y" junction structure to trigger a restriction endonuclease-aided target recycling. The target recycling resulted in the release of biotin labeled to the immobilized DNA from the nanosheet-modified electrode, thus decreased the consumption of hydrogen peroxide by horseradish peroxidase-mediated electrochemical reduction after binding the left biotin with horseradish peroxidase-labeled streptavidin, which produced an increasing photoelectrochemical response. The 'signal on' strategy for photoelectrochemical detection of DNA showed a low detection limit down to the subfemtomole level and good specificity to single-base mismatched oligonucleotides. The sensitized porous ZnO nanosheets are promising for applications in both photovoltaic devices and photoelectrochemical biosensing.

Received 7th September 2013
Accepted 27th November 2013

DOI: 10.1039/c3nr04777f

www.rsc.org/nanoscale

Introduction

Zinc oxide (ZnO), as an important wide band gap semiconducting material, possesses many useful properties such as piezoelectricity, optical absorption and emission, high voltage–current nonlinearity, sensitivity to gases and chemical agents, and catalytic activity.[1,2] Considerable efforts have been devoted to produce various ZnO morphologies, such as nanowires, nanosheets, nanorods, and porous and comb-like nanostructures.[3,4] Among these structures, porous ZnO nanosheets have attracted extensive attention. The porous nanostructures are expected not only to exhibit high light-collection efficiency and a fast motion of charge carriers[5,6] but also to provide efficient transport pathways to reactant and product molecules,[7] which offer benefits for applications in the fields of gas sensing, lithium-ion battery, selective adsorption, photovoltaic, and photocatalysis.[8–10] However, the wide band gap of ZnO suffers from the major limitation of weak visible light absorption.[11] Sensitizing metal oxide with small band gap semiconductors is one of the most promising approaches to increase their visible light absorption.[12] These hybrid or multi-semiconductor systems can promote the separation of electron–hole pairs and enhance photoelectrochemical performance,[13] which has led to significant interest in the fabrication of various ZnO-semiconductor nanocomposites, including TiO_2 nanotubes,[14] CdS,[15] ZnO/Cu_2O thin film,[16] CdSe QDs sensitized single-crystal ZnO nanowires[17] and CdS/ZnO nanotube arrays.[18] Although the above photoelectrochemical platforms exhibit good performance for the detection of biomolecules, their applications are limited in biological systems due to the ultraviolet light irradiation. This work used CdTe QDs as a new sensitizer to synthesize the functional porous ZnO nanosheets. This nanosheets showed an excellent visible-light absorbency and photoelectrochemical activity.

CdTe has a high optical absorption coefficient (>10^4 cm^{-1}) and narrow band gap of ~1.5 eV,[19] matching the preferred range of the solar radiation spectrum.[20] The appropriate band alignment between CdTe QDs and ZnO allows efficient charge carrier

[a]*State Key Laboratory of Analytical Chemistry for Life Science, School of Chemistry and Chemical Engineering, Nanjing University, Nanjing 210093, P.R. China. E-mail: jpl@nju.edu.cn*

[b]*Institute of Basic Medicine, Shandong Academy of Medical Sciences, Jinan 250062, P.R. China*

injection.[21] In addition, it has been shown that semiconductor nanomaterials can generate multiple charge carriers with a single photon, which improves the efficiency of the device.[22,23] Therefore, the ZnO/CdTe nanohybrids on a transparent conductive substrate would hold great potential for a number of photoelectrical applications. For example, a nanostructured photoelectrode fabricated by electrochemical deposition of CdTe on a vertically aligned ZnO nanorod at indium tin oxide (ITO) has shown good photovoltaic properties.[20] A CdTe/ZnO nanocomposite thin film with varied semiconductor-phase extended structures has been designed to produce an enhancement in the photo-induced current by using radio frequency sputter deposition technique.[24] However, most of the reports focus on their applications in photovoltaics,[25] optoelectronics,[26] as photoanodes,[27] and as gas sensors.[28] Here the photoelectrochemical behavior of ZnO/CdTe nanohybrids was studied for the first time, and a photoelectrochemical biosensor prepared with CdTe QD-functionalized porous ZnO nanosheets was proposed.

The functional porous ZnO nanosheets were synthesized by using a silylating reagent to introduce the amino groups on the surface of ZnO nanosheets and then covalently binding the CdTe QDs capped with 3-mercaptopropionic acid to these amine groups *via* amidation (Scheme 1A). The CdTe/ZnO nanohybrids showed a substantially enhanced photocurrent in the visible light range due to the appropriate band alignment between CdTe QDs and ZnO, the porous structure of ZnO nanosheet and the high loading density of CdTe QDs.[29–31] The efficient photoelectrochemical performance involved the participation of hydrogen peroxide (H_2O_2) as an electron acceptor. Thus the functional porous ZnO nanosheets could be used for design of hydrogen peroxide-related biosensors by monitoring the formation or consumption of hydrogen peroxide. In this work a photoelectrochemical DNA biosensor was designed by immobilizing a biotin-labeled DNA capture probe on the nanosheet-modified electrode to recognize target DNA and an assistant DNA, which produced a "Y" junction structure to trigger a restriction endonuclease-aided target recycling for taking out the immobilized biotin (Scheme 1B). The target recycling decreased the amount of biotin and thus the consumption of hydrogen peroxide by horseradish peroxidase-mediated electrochemical reduction after binding the left biotin with horseradish peroxidase-labeled streptavidin. The "signal on" photoelectrochemical biosensor achieved highly sensitive detection of DNA down to the subfemtomole level, indicating a promising application of the functional porous ZnO nanosheets in bioanalysis.

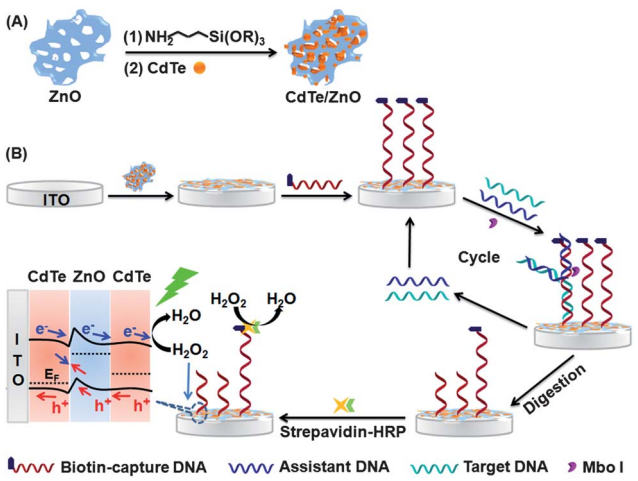

Scheme 1 Schematic representation of (A) the synthesis of the CdTe/ZnO nanohybrids, and (B) the construction and photoelectrochemical strategy of the DNA biosensor.

Experimental

Materials and reagents

Zinc acetate and urea were purchased from Shanghai Chemical Co. (China). 3-Mercaptopropionic acid (MPA, ≥99%), *N*-hydroxysulfosuccinimide (NHS) and 1-ethyl-3-(3-dimethylaminopropyl) carbodiimide (EDC) were purchased from Sigma-Aldrich Chemical Co. (St. Louis, MO, U.S.A.). FastDigest enzyme MboI and 10× FastDigest buffer were obtained from Promega Co. (U.S.A.). Streptavidin–peroxidase was supplied by Wuhan Boster Biological Technology Ltd. Monoethanolamine (MEA) was purchased from Sinopharm Chemical Reagent Co., Ltd. (Shanghai, China). (3-Aminopropyl)triethoxysilane (APTES) and cadmium chloride ($CdCl_2 \cdot 2.5H_2O$) were purchased from Alfa Aesar China Ltd. (China). ITO coated glass as the electrode material was purchased from Zhuhai Kaivo Electronic Components Co., Ltd. Ultrapure water obtained from a Millipore water purification system (≥18 MΩ, Milli-Q, Millipore) was used in all assays.

0.1 M phosphate buffered salines (PBS) of various pHs were prepared by mixing the stock solutions of 0.1 M NaH_2PO_4 and Na_2HPO_4 containing 0.1 M KNO_3. The washing buffer was 0.05% (w/v) Tween-20 (PBST) in 0.01 M pH 7.4 PBS. Tris (hydroxymethyl) aminomethane (Tris)–HCl (10 mM, pH 7.4) containing 1 mM ethylenediaminetetraacetic acid (EDTA) and 50 mM NaCl was used as a DNA immobilization buffer. Tris–HCl (0.1 M) was employed as a detection electrolyte during the photoelectrochemical procedure, and was deaerated with highly pure nitrogen prior to the photoelectrochemical measurements.

The oligonucleotides were purchased from Sangon Biological Engineering Technology Co. Ltd. (Shanghai, China) and purified using high-performance liquid chromatography. Their sequences were as follows: capture probe: 5′-biotin-AAA-AGA-TCA-AAC-TTC-TCG-ATT-TTT-TTT-TT-C_6NH_2-3′; assistant probe: 5′-ACA-GCA-CGC-CTT-TGA-TC-3′; target: 5′-TCG-AGA-AGG-GCG-TGC-TGT-AA-3′; single-base mismatched oligonucleotide: 5′-TCG-AGA-AGG-GCC-TGC-TGT-AA-3′; three-base mismatched oligonucleotide: 5′-TCG-TGA-AGG-GGG-TGC-TCT-AA-3′.

Apparatus

Photoluminescence (PL) and UV-Vis absorption spectra were recorded on a RF-5301 PC fluorometer (Shimadzu Co., Japan) and a Shimadzu UV-3600 UV-Vis-NIR photospectrometer (Shimadzu Co., Japan), respectively. Attenuated total reflection

Fourier transform IR (ATR-FTIR) spectra were recorded on a Vector 22 Fourier transform infrared spectrometer (Bruker Optics, Germany). X-ray photoelectron spectral (XPS) experiments were operated on an ESCALAB 250 spectrometer (Thermo-VG Scientific Co., U.S.A.) with an ultrahigh vacuum generator. X-ray diffraction (XRD) was measured on Philips X'pert Pro X-ray diffractometer with Cu Ka radiation of 1.542 Å. Scanning electron microscopic (SEM) images were obtained using a Hitachi S-4800 scanning electron microscope (Japan). High resolution transmission electron microscopy (TEM) with energy dispersive X-ray analysis (EDX) was performed at 200 kV using a JEM-2100 TEM (JEOL, Japan). Photoelectrochemical detection was performed on Controlled Intensity Modulated Photo Spectrometer (Zahner Zennium, German) with a LW619 LED light (wavelength at 505 nm) as the accessory light source. All experiments were carried out at room temperature using a conventional three-electrode system with a modified ITO electrode as the working electrode, a platinum wire as the auxiliary electrode, and a saturated calomel electrode (SCE) as the reference electrode.

Preparation of the QDs

The CdTe QDs were prepared following the method reported earlier.[32,33] Briefly, the Cd precursor solutions were prepared by mixing a solution of $CdCl_2$ and stabilizer (MPA) solution, and then adjusted to pH 8.5 with 0.5 M NaOH. The typical molar ratio of Cd : Te : MPA was 2 : 1 : 4.8 in our experiments. Under vigorous stirring, the prepared oxygen-free NaHTe solution was injected. The resulting mixture solution was heated to 99–100 °C and refluxed for some time to obtain the QDs. The as-prepared QDs solution was precipitated with an equivalent amount of acetone and collected by centrifugation. The colloidal precipitate was redissolved in ultrapure water to the original volume.

Preparation of porous ZnO nanosheets

In a typical synthesis,[28] 25 mL of 0.2 M zinc acetate solution was added into 25 mL of 0.4 M urea solution drop by drop. The mixture was then kept in the microwave system under stirring at 95 °C for 30 min. The resultant precipitate was then centrifuged, washed, and dried at 80 °C. Finally, ZnO porous nanosheets were obtained by annealing the precursor at 400 °C for 2 h in air atmosphere.

Preparation of CdTe/ZnO

The hierarchical structure of CdTe/ZnO was prepared according to a method described in the literature with some modifications.[34] First, the as-prepared porous ZnO nanosheet was functionalized with amine groups. An amount of 0.01 g of the ZnO in powder form was dispersed in 10 mL of an ethanol–water mixture (95%/5% V/V). The pH value of the solution was adjusted to 5 by dropping in acetic acid. After the addition of 600 μL of APTES, the suspension was sonicated for 20 min, and transferred into an oven at 75 °C for 1 h. The suspension was finally centrifuged and washed with ethanol three times to remove the unreacted silane. The obtained sample was named APTES/ZnO. Second, the CdTe QDs were bound to the APTES/ZnO surface by using the following procedure: the obtained APTES/ZnO was dispersed in 10 mL of ultrapure water and sonicated for 15 min. Different volumes of CdTe suspension were added to the APTES/ZnO dispersion (pH = 7.0), and the mixtures were stirred for 20 h at room temperature. Then the powders were centrifuged and washed with ultrapure water to remove the unreacted CdTe nanocrystals. The obtained samples were named as CdTe/ZnO.

Preparation of the biosensor and DNA detection

After an ITO electrode was cleaned with NaOH (1 M) and H_2O_2 (10%), washed with acetone and twice-ultrapure water, and dried at room temperature, 20 μL of the CdTe/ZnO stock solution was coated onto the ITO electrode and dried at room temperature to obtain an CdTe/ZnO/ITO electrode. Then the CdTe/ZnO/ITO electrodes were immersed in a solution containing 10 mM EDC and 20 mM NHS for 50 min at room temperature. After rinsing, 20 μL of 1 μM capture DNA was dropped onto the surface of the electrode and incubated at 4 °C overnight. The as-prepared electrode was washed thoroughly to remove the unlinked capture DNA before the blocking with 1 mM MEA at 4 °C for 2 h and final rinsing. Then the mixture of 1 μM assistant probe, 0.1 U μL^{-1} enzyme and target at different concentrations was added and incubated for 60 min at 37 °C and then washed with PBST.

Finally, 20 μL streptavidin labeled peroxidase (20 μg mL^{-1}) was dropped onto the surfaces and incubated for 40 min, then washed with PBST to remove the unbound tags. The photoelectrochemical measurements were performed with light excitation of 505 nm at the applied potential of −0.20 V *versus* SCE in 0.1 M Tris–HCl solution containing 0.5 mM H_2O_2.

Results and discussion

Characterization of CdTe QD-functionalized porous ZnO nanosheets

The SEM image of the obtained ZnO nanosheets displayed a plate-like nanostructure with nanometer-sized porous architecture (Fig. 1A). The TEM image showed the random pores in the nanosheets (Fig. 1B). The distinct peaks in its XRD pattern suggested a hexagonal crystal structure for the porous ZnO nanosheets (JCPDS card no. 36-1451) (Fig. 2A). Moreover, no other secondary or amorphous phase was observed, indicating the high purity of the ZnO nanosheets.

The UV-Vis absorption spectrum of MPA-capped CdTe QDs showed a wide absorption band with an absorption shoulder around 627 nm (Fig. 2B, curve a). Their size and the concentration of the QDs solution could be estimated to be 3.95 nm and 1.16 μM using the empirical equations as follows:[35]

$$D = (9.8127 \times 10^{-7})\lambda^3 - (1.7147 \times 10^{-3})\lambda^2 + (1.0064)\lambda - 194.84$$

$$C = \frac{A}{10043(D)^{2.12}L}$$

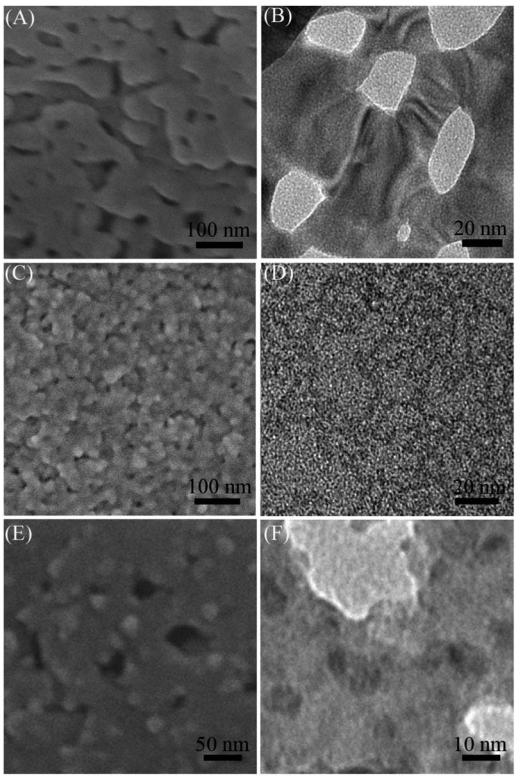

Fig. 1 High resolution SEM and TEM images of (A) and (B) porous ZnO nanosheets, (C) and (D) CdTe QDs, and (E) and (F) CdTe/ZnO nanohybrids.

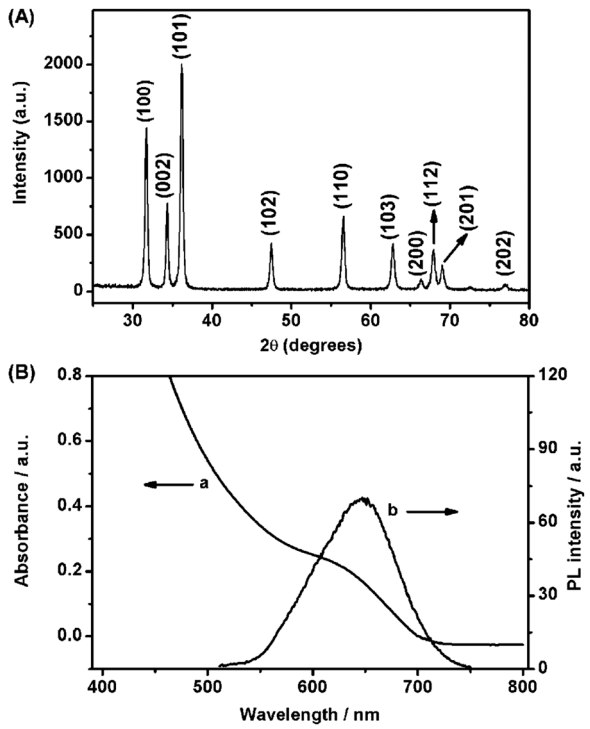

Fig. 2 (A) XRD patterns of the porous ZnO nanosheets, and (B) UV-Vis absorption (a) and fluorescence (b) spectra of MPA-CdTe QDs.

where D (nm) and C (mol L^{-1}) are the size and concentration of CdTe QDs, λ (nm) is wavelength of the first excitonic absorption peak, A is the absorbance at the peak position of the first exciton absorption peak for a given sample, and L (cm) is the path length of the radiation beam.

The fluorescent spectrum of the CdTe QDs showed a strong emission peak at 642 nm (Fig. 2B, curve b), which is consistent with the UV-Vis absorption inflection point, indicating the band gap emission of the CdTe QDs core. After CdTe QDs were covalently attached to the surface of porous ZnO nanosheets *via* amidation, the CdTe QDs could be clearly seen from both the high resolution SEM and TEM images (Fig. 1E and F). The EDX spectrum showed the signals of Cd, Te and Zn with the molar ratio of ~1.5 : 1 : 4.4, which confirmed the formation of CdTe/ZnO nanohybrids. Compared with the aggregate size of the CdTe QDs film (Fig. 1C and D), the aggregation of CdTe QDs in the nanohybrids was obviously reduced, which was favorable for improving the photoelectrochemical efficiency.

The UV-Vis diffuse reflectance spectrum of the porous ZnO nanosheets did not show any absorbance in the visible wavelength range, and the increased absorptive profile occurred over wavelengths less than 430 nm, which reached a absorbance plateau at 350 nm (Fig. 3A, curve a). After the ZnO nanosheets were modified with CdTe QDs, the absorption extended to the visible region (Fig. 3A, curve b), which indicated that the ZnO nanosheets were successfully sensitized by the CdTe QDs.

The survey XPS spectrum of the porous ZnO nanosheets showed the Zn and O peaks (Fig. 3B, curve a). Compared with 404.5 eV of Cd 3d5 in pure CdTe, the binding energy of Cd 3d5 in the functional nanosheets shifted to 404.8 eV (Fig. 3C), which confirmed the phase interaction between CdTe and ZnO. In addition, the binding energy of O1s split into four parts with peak values of 529.8, 530.5, 531.5 and 531.7 eV, respectively (Fig. 3D). The peak at 531.7 eV (C═O) indicated the loading of CdTe QDs on ZnO nanosheets. The binding energy shift of Te

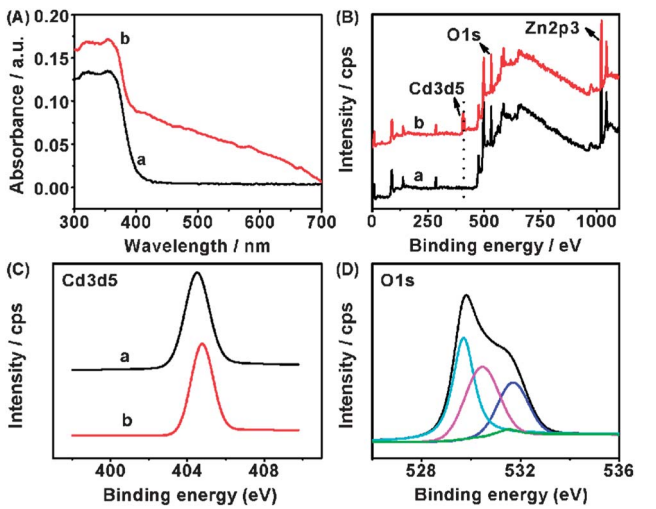

Fig. 3 (A) UV-Vis, (B) survey and (c) Cd3d5 XPS spectra of porous ZnO nanosheets (a) and CdTe/ZnO nanohybrids (b). (D) is O1s XPS spectra of CdTe/ZnO nanohybrids.

3d5 was not emphasized due to the overlap of Te and Zn. The atomic ratio of Zn 2p3 and Cd 3d5 is about 6.0 from the XPS data, which indicated that the bifunctional linker molecule could successfully improve the loading density of CdTe QDs.

Fluorescence microscopic imaging was performed to further confirm the architecture of the functional nanosheets. As shown in Fig. 4, the homogenous red fluorescence spots of the functional nanosheets were observed on the substrate, indicating the good conjugation between the CdTe QDs and ZnO nanosheets.

Photoelectrochemical behavior of CdTe QD-functionalized porous ZnO nanosheets

To clarify the effect of the ratio of CdTe QDs to ZnO nanosheets on the photoelectrochemical properties of the hybrids, three different CdTe/ZnO nanohybrids with the ratios of 1 : 10, 1 : 2 and 1 : 1 (V/V) were prepared. Photocurrent measurement was introduced to investigate the effect of CdTe on the nanohybrids. The photocurrent density of the CdTe/ZnO nanohybrid films increased with the increasing content of CdTe QDs (Table 1). When the ratio of CdTe QDs to ZnO was set at 1 : 2 (V/V), the photocurrent density was the same as that with a ratio of 1 : 1 (V/V), suggesting that the CdTe QDs in the nanohybrids reached saturation after the CdTe/ZnO ratio of 1 : 2 (V/V).

The photoelectrochemical behaviors of the MPA-capped CdTe QDs, porous ZnO nanosheets and CdTe QDs functionalized porous ZnO nanosheets were compared to further confirm the effect of CdTe QDs on the photoelectrochemical properties of the nanohybrids. As shown in Fig. 5, under the irritation with visible light at 505 nm, the pure ZnO nanosheets did not show significant photocurrent signals (curve a), while the CdTe QDs generated a cathodic photocurrent (curve b), indicating a p-type material.[36] After the porous ZnO nanosheets were modified with CdTe QDs, the nanohybrids exhibited 2.2 times the photocurrent density of the CdTe QDs. Considering the presence of CdTe QDs on both sides of ZnO nanosheets as an n-type material, the prepared CdTe/ZnO nanohybrids produced a pnp junction-like structure, in which the contact between ZnO and CdTe could bend their Fermi levels (EF) to fit each other and allow efficient charge carrier injection.[37–39] Therefore, under visible light irradiation, the CdTe/ZnO nanohybrid-modified ITO electrode results in the enhanced photocurrent by using H_2O_2 as electron acceptor.

The dependence of the photocurrent density on the concentration of H_2O_2 was investigated in Fig. 6A. The photocurrent density increases with increasing the concentration of H_2O_2 up to 1.0 mM, and then slightly decreases with further elevation of the concentration of H_2O_2 due to the H_2O_2-mediated oxidation of the surface of the CdTe QDs.[40–42] This property led to a novel methodology for the design of H_2O_2-related biosensors by the formation or consumption of H_2O_2.

Here, using biotin-labeled DNA as a capture probe, a model biosensor was proposed by immobilizing the probe on the CdTe/ZnO nanosheet-modified electrode *via* amidation to recognize the target DNA in the presence of an assistant DNA (Scheme 1B), which produced a "Y" junction structure to trigger a restriction endonuclease-aided target recycling for signal amplification. The target recycling resulted in the release of biotin labeled to the capture DNA from the CdTe/ZnO nanosheet-modified electrode, reduced the binging sites for horseradish peroxidase-labeled streptavidin, and thus decreased the consumption of H_2O_2 by horseradish peroxidase-mediated electrochemical reduction. Therefore, with increases of the target DNA concentration, an increasing photoelectrochemical response could be obtained by using H_2O_2 as an electron acceptor. The "signal on" photoelectrochemical strategy should achieve a highly sensitive detection of DNA.

Table 1 Effect of the ratios of CdTe/ZnO on photocurrent intensity

No.	Ratios of CdTe/ZnO (V/V)	Photocurrent density (j, nA cm^{-2})
1	1 : 10	325
2	1 : 2	1340
3	1 : 1	1375

Optimization of conditions

To obtain good performance in photoelectrochemical DNA detection, several experimental parameters were optimized including the amount of nanohybrids used for modification, the concentration of capture DNA, and the incubation time of

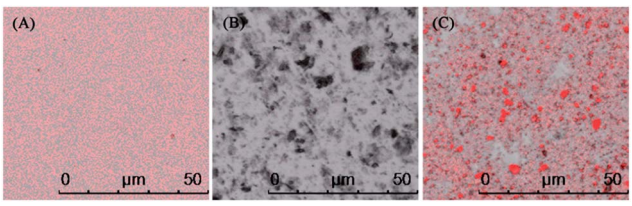

Fig. 4 Fluorescence microscopic image of CdTe (A), ZnO (B), CdTe/ZnO (C).

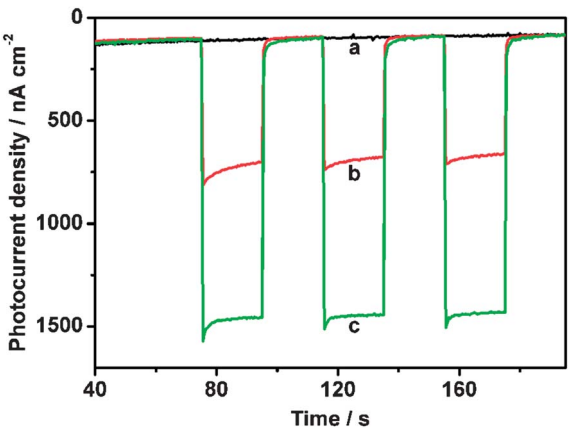

Fig. 5 Photocurrent responses of (a) ZnO, (b) CdTe, and (c) CdTe/ZnO-modified ITO electrodes in 0.1 M Tris–HCl (pH = 7.4) containing 0.5 mM H_2O_2. Light excitation of 505 nm is switched every 20 s and the applied potential is −0.20 V.

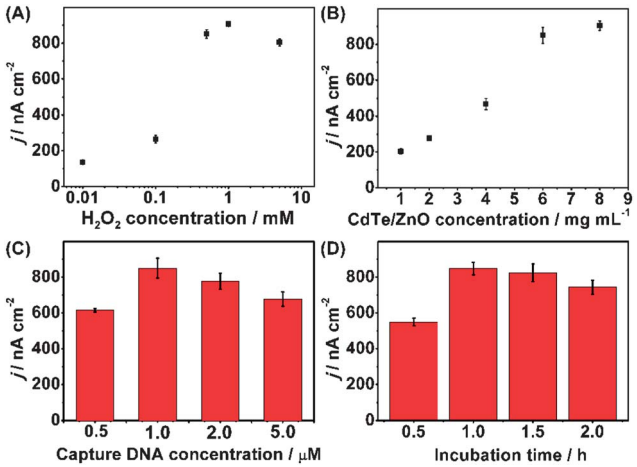

Fig. 6 Effects of (A) H_2O_2 concentration, (B) CdTe/ZnO concentration, (C) capture DNA concentration and (D) incubation time on photocurrent responses of the biosensor (error bar results from three independent electrodes).

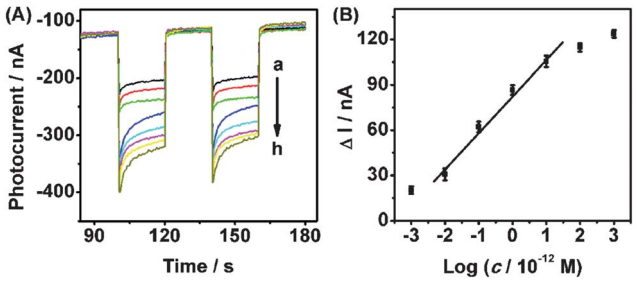

Fig. 7 (A) Photocurrent responses of the biosensor at different concentrations of target DNA. (B) The corresponding calibration curve ($\Delta I = I - I_0$, and I_0 and I are the photocurrents of capture DNA/CdTe/ZnO/ITO without and with target DNA, respectively).

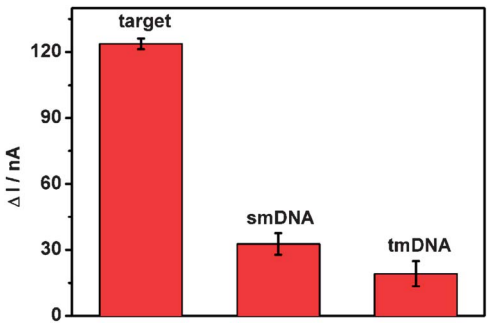

Fig. 8 Photocurrent changes at 1 nM of perfect complementary sequence, single-base mismatched sequence and three-base mismatched sequence targets.

hybridization. The photocurrent density of the electrode essentially depends on the amount of CdTe/ZnO nanohybrids (Fig. 6B). With an increase of CdTe/ZnO density, the photocurrent is enhanced and then reaches a plateau when 6 mg mL^{-1} CdTe/ZnO is cast onto the ITO electrode. Although more CdTe/ZnO could increase the nanohybrids' density on the electrode surface, the photocurrent density does not obviously increase, which is attributed to the increasing film thickness that inhibits the electron exchange. Since the photocurrent intensity of 6 mg mL^{-1} QDs is 95.7% of the intensity at 8 mg mL^{-1} and strong enough for sensitive detection, 6 mg mL^{-1} of CdTe/ZnO is chosen for the preparation of the biosensor.

Generally, the density of the biotin-labeled capture probes on electrodes increases with increasing of the capture probes concentration, which strongly affects the performance of the proposed biosensor for the detection of the target DNA.[43] At low surface density, it would capture few target DNA strands and it is hard to get a considerable photocurrent change. However, at high density, the sensitivity may be in fact decreased because the efficiency of DNA hybridization is low due to steric effects.[44] The photocurrent density increases greatly with an increasing concentration of capture DNA from 0.5 to 1 μM and then decreases when the concentration is increased beyond 1 μM (Fig. 6C). So we employ 1 μM as the optimized concentration of the capture probes. On the other hand, incubation time also influences the sensitivity of this biosensor. The photocurrent density reaches nearly a plateau after 1 h in the presence of 1 pM target (Fig. 6D). In order to ensure the large photocurrent, 1 h is chosen as the optimal reaction time.

Analytical performance of the photoelectrochemical biosensor

Photoelectrochemical detection is carried out in 0.1 M Tris–HCl (pH = 7.4) containing 0.5 mM H_2O_2. With the increasing of the target DNA concentration, the consumption of hydrogen peroxide decreased. Thus a 'signal on' photoelectrochemical strategy is achieved for the detection of DNA. Under the optimal conditions, different concentrations of target DNA are introduced. As shown in Fig. 7A, the photocurrent intensity increases with the increasing concentration of target DNA. Hence the quantitative behavior of the photoelectrochemical hybridization assay could be assessed by measuring the change of photocurrent intensity before and after incubating with target DNA. From Fig. 7B, a linear range is achieved from 1.0×10^{-11} to 1.0×10^{-14} M with a correlation coefficient of 0.993. The detection limit at a signal-to-noise ratio of 3 is 9.3×10^{-16} M, which is much lower than the 0.3 nM of the Pd nanowires-based fluorescent detection method,[45] 1.3×10^{-12} M of the three-input DNA logic gate systems[46] and 2.9×10^{-13} M of a graphene-based electrochemical DNA biosensor.[47]

Selectivity is also an important parameter for a biosensor. Different kinds of DNA sequences including a perfect complementary target, single-base mismatched oligonucleotide (smDNA) and three-base of mismatched oligonucleotide (tmDNA) are chosen to investigate the selectivity of this biosensor at the same concentration (1 nM). As shown in Fig. 8, the signal for perfect complementary target is 3.8-folds of smDNA and 6.5-folds of tmDNA, indicating the biosensor exhibits good performance to discriminate perfect complementary target and the base mismatched oligonucleotides, which should be attributed to the specific cleaving site of the

"Y" junction structure. The high specificity of this method provides a possibility for the potential application of this sensor in real samples.

Conclusions

The high density CdTe/ZnO nanohybrids are successfully synthesized through a facile method by using a linker molecule to covalently bind CdTe QDs with the porous ZnO nanosheets. The functional nanosheets showed an excellent visible-light absorbency and much higher photoelectrochemical activity than both CdTe QDs and ZnO nanosheets due to the three possible reasons: (1) the appropriate band alignment between CdTe QDs and ZnO nanosheets; (2) the interconnected two-dimensional porous structure of ZnO nanosheets which facilitates the transportation of reactants and products through the interior space, and favors the harvesting of exciting light due to the enlarged surface area and multiple scattering within the porous framework; (3) the high loading density of CdTe QDs on the nanosheets. Furthermore, the CdTe/ZnO nanosheet-modified electrode showed a sensitive photocurrent response to hydrogen peroxide as an electron acceptor, thus leading to a novel methodology for design of a hydrogen peroxide-related photoelectrochemical platform by the formation or consumption of hydrogen peroxide. Coupling the biological amplification strategy, the proposed photoelectrochemical approach shows a good performance in terms of high sensitivity, low detection limit, wide detection range and no requiring of specific sequences for detection of DNA. The sensitized porous ZnO nanosheets open a new avenue for the construction of a universal platform for photovoltaic devices and photoelectrochemical biosensors.

Acknowledgements

This work was financially supported by the National Basic Research Program of China (2010CB732400), National Natural Science Foundation of China (21075060, 21135002, 21121091, 21375060), and the program for New Century Excellent Talents in University (NCET100479).

Notes and references

1 D. C. Look, *Mater. Sci. Eng., B*, 2001, **80**, 383.
2 Z. R. Tian, J. A. Voigt, J. Liu, B. Mckenzie, M. J. Mcdermott, M. A. Rodriguez, H. Konishi and H. F. Xu, *Nat. Mater.*, 2003, **2**, 821.
3 Q. F. Zhang, C. S. Dandeneau, X. Y. Zhou and G. Z. Cao, *Adv. Mater.*, 2009, **21**, 4087.
4 F. Xu and L. T. Sun, *Energy Environ. Sci.*, 2011, **4**, 818.
5 F. Lu, W. P. Cai and Y. G. Zhang, *Adv. Funct. Mater.*, 2008, **18**, 1047.
6 Q. J. Xiang, K. L. Lv and J. G. Yu, *Appl. Catal., B*, 2010, **96**, 557.
7 J. G. Yu, J. J. Fan and B. Cheng, *J. Power Sources*, 2011, **196**, 7891.
8 M. Chen, Z. H. Wang, D. M. Han, F. B. Gu and G. S. Guo, *J. Phys. Chem. C*, 2011, **115**, 12763.
9 S. W. Liu, C. Li, J. G. Yu and Q. J. Xiang, *CrystEngComm*, 2011, **13**, 2533.
10 S. Dilger, C. Lizandara-Pueyo, M. Krumm and S. Polarz, *Adv. Mater.*, 2012, **24**, 543.
11 R. S. Devan, R. A. Patil, J. H. Lin and Y. R. Ma, *Adv. Funct. Mater.*, 2012, **22**, 3326.
12 J. Hensel, G. M. Wang, Y. Li and J. Z. Zhang, *Nano Lett.*, 2010, **10**, 478.
13 X. W. Wang, G. Liu, Z. G. Chen, F. Li, L. Z. Wang, G. Q. Lu and H. M. Cheng, *Chem. Commun.*, 2009, 3452.
14 D. Chen, H. Zhang, X. Li and J. H. Li, *Anal. Chem.*, 2010, **82**, 2253.
15 W. W. Zhao, X. Y. Dong, J. Wang, F. Y. Kong, J. J. Xu and H. Y. Chen, *Chem. Commun.*, 2012, **48**, 5253.
16 A. T. Marin, D. Muñoz-Rojas, D. C. Iza, T. Gershon, K. P. Musselman and J. L. MacManus-Driscoll, *Adv. Funct. Mater.*, 2013, **23**, 3413.
17 K. S. Leschkies, R. Divakar, J. Basu, E. Enache-Pommer, J. E. Boercker, C. B. Carter, U. R. Kortshagen, D. J. Norris and E. S. Aydil, *Nano Lett.*, 2007, **7**, 1793.
18 X. P. Qi, G. W. She, Y. Y. Liu, L. X. Mu and W. S. Shi, *Chem. Commun.*, 2012, **48**, 242.
19 S. Shokhovets, O. Ambacher and G. Gobsch, *Phys. Rev. B: Condens. Matter Mater. Phys.*, 2007, **76**, 125203.
20 X. N. Wang, H. J. Zhu, Y. M. Xu, H. Wang, Y. Tao, S. K. Hark, X. D. Xiao and Q. Li, *ACS Nano*, 2010, **4**, 3302.
21 C. G. Van de Walle and J. Neugebauer, *Nature*, 2003, **423**, 626.
22 R. D. Schaller and V. I. Klimov, *Phys. Rev. Lett.*, 2004, **92**, 186601.
23 R. J. Ellingson, M. C. Beard, J. C. Johnson, P. R. Yu, O. I. Micic, A. J. Nozik, A. Shabaev and A. L. Efros, *Nano Lett.*, 2005, **5**, 865.
24 R. J. Beal, J. B. Kana Kana and B. G. Potter, Jr, *Appl. Phys. Lett.*, 2012, **101**, 031102.
25 T. C. Kaspar, T. Droubay and J. E. Jaffe, *Appl. Phys. Lett.*, 2011, **99**, 263504.
26 B. G. Potter, Jr, R. J. Beal and C. G. Allen, *J. Appl. Phys.*, 2012, **111**, 034305.
27 X. N. Wang, R. Liu, T. Wang, B. Y. Wang, Y. Xu and H. Wang, *ACS Appl. Mater. Interfaces*, 2013, **5**, 3312.
28 Z. Jing and J. Zhan, *Adv. Mater.*, 2008, **20**, 4547.
29 J. G. Yu, J. C. Yu, M. K. P. Leung, W. K. Ho, B. Cheng, X. J. Zhao and J. C. Zhao, *J. Catal.*, 2003, **217**, 69.
30 J. Zhang, J. G. Yu, Y. M. Zhang, Q. Li and J. R. Gong, *Nano Lett.*, 2011, **11**, 4774.
31 P. V. Kamat, *J. Phys. Chem. C*, 2008, **112**, 18737.
32 M. Y. Gao, S. Kirstein, H. Möhwald, A. L. Rogach, A. Kornowski, A. Eychmüller and H. Weller, *J. Phys. Chem. B*, 1998, **102**, 8360.
33 J. S. W. Mak, A. A. Farah, F. F. Chen and A. S. Helmy, *ACS Nano*, 2011, **5**, 3823.
34 D. Costenaro, F. Carniato, G. Gatti, C. Bisio and L. Marchese, *J. Phys. Chem. C*, 2011, **115**, 25257.
35 W. W. Yu, L. H. Qu, W. Z. Guo and X. G. Peng, *Chem. Mater.*, 2003, **15**, 2854.

36 M. Moriya, T. Minegishi, H. Kumagai, M. Katayama, J. Kubota and K. Domen, *J. Am. Chem. Soc.*, 2013, **135**, 3733.
37 J. Y. Cao, J. J. Xing, Y. J. Zhang, H. Tong, Y. P. Bi, T. Kako, M. Takeguchi and J. H. Ye, *Langmuir*, 2013, **29**, 3116.
38 L. Jing, J. Velasco Jr, P. Kratz, G. Liu, W. Z. Bao, M. Bockrath and C. N. Lau, *Nano Lett.*, 2010, **10**, 4000.
39 M. J. Deen, S. Rumyantsev, R. Bashir and R. Taylor, *J. Appl. Phys.*, 1998, **84**, 625.
40 X. Y. Li, Y. L. Zhou, Z. Z. Zheng, X. L. Yue, Z. F. Dai, S. Q. Liu and Z. Y. Tang, *Langmuir*, 2009, **25**, 6580.
41 M. C. Mancini, B. A. Kairdolf, A. M. Smith and S. M. Nie, *J. Am. Chem. Soc.*, 2008, **130**, 10836.
42 R. Gill, L. Bahshi, R. Freeman and I. Willner, *Angew. Chem., Int. Ed.*, 2008, **47**, 1676.
43 U. Rant, K. Arinaga, S. Fujita, N. Yokoyama, G. Abstreiter and M. Tornow, *Langmuir*, 2004, **20**, 10086.
44 J. Zhang, S. P. Song, L. Y. Zhang, L. H. Wang, H. P. Wu, D. Pan and C. H. Fan, *J. Am. Chem. Soc.*, 2006, **128**, 8575.
45 L. B. Zhang, S. J. Guo, S. J. Dong and E. K. Wang, *Anal. Chem.*, 2012, **84**, 3568.
46 X. M. Li, T. R. Ding, L. Sun and C. M. Mao, *Biosens. Bioelectron.*, 2011, **30**, 241.
47 W. Sun, Y. Y. Zhang, A. H. Hu, Y. X. Lu, F. Shi, B. X. Lei and Z. F. Sun, *Electroanalysis*, 2013, **25**, 1417.